

Cooperative Edge Caching with Large Language Model in Wireless Networks

Ning Yang, *Member, IEEE*, Wentao Wang, Lingtao Ouyang, and Haijun Zhang, *Fellow, IEEE*

Abstract—Cooperative edge caching within spatially overlapping coverage zones introduces intricate coupling among Base Station (BS) caching decisions, rendering online content replacement highly sensitive to both spatial topology and temporal content reuse. Conventional heuristics often suffer from myopia, while Deep Reinforcement Learning agents typically rely on brittle numerical state/action representations and necessitate computationally prohibitive retraining under topological or traffic dynamics. This paper proposes a Large Language Model (LLM)-based multi-BS caching orchestrator, where the LLM functions as the sole autonomous decision engine, interacting with the environment via a rigorously validated text-to-action interface. At each time slot, the environmental state is deterministically rendered into a prompt encapsulating the cache inventory of each BS, the current set of deduplicated requests, and multi-scale frequency summaries. The LLM is tasked with generating exactly one decision line per BS, which is subsequently parsed and strictly verified against feasibility constraints. We align the LLM through a two-stage training paradigm: initially performing completion-only Supervised Fine-Tuning on lookahead oracle trajectories to acquire action syntax and robust initialization, followed by Group Relative Policy Optimization. The latter employs an “opportunity-aware” reward mechanism, utilizing the multi-step cooperative hit rate gain relative to a no-operation (NoOp) baseline as the primary signal, alongside explicit penalties for invalid outputs. Under a frozen-trajectory evaluation protocol that reuses identical request traces and association graphs across methods, the proposed orchestrator approaches a single-step exhaustive-search oracle (0.610 vs. 0.617 in a standard 5-BS scenario), surpasses classical baselines (e.g., +4.1% over least-frequently used), and exhibits robust zero-shot transfer across cache capacity, library size, popularity skewness, and user density.

Index Terms—Edge caching, large language models, supervised fine-tuning, GRPO, strict action parsing, unified evaluation.

I. INTRODUCTION

MOBILE data traffic in 5G and emerging 6G systems continues to increase rapidly due to the proliferation of video streaming, interactive applications, and AI-generated content, placing sustained pressure on backhaul capacity and cloud infrastructures [1], [2]. Edge caching alleviates this burden by proactively placing frequently requested content in Base Station (BS) storage, enabling local service with

Ning Yang is with the Institute of Automation, Chinese Academy of Sciences, Beijing, 100190, China (e-mail: ning.yang@ia.ac.cn).

Wentao Wang is with the Leicester International Institute, Dalian University of Technology, Dalian, Liaoning, 124221, China (e-mail: shiyanxi1@mail.dlut.edu.cn).

Lingtao Ouyang is with the School of Management, Xi'an Jiaotong University, Xi'an, Shaanxi, 710049, China (e-mail: 2386558088@stu.xjtu.edu.cn).

Haijun Zhang is with the School of Computer and Communication Engineering, University of Science and Technology Beijing, Beijing, 100083, China (e-mail: zhanghaijun@ustb.edu.cn).

reduced latency and reduced backhaul load [3], [4]. While early research focused on isolated or non-overlapping cells, modern heterogeneous deployments are increasingly user-centric: coverage regions of multiple BSs overlap, and users may be served by different BS subsets over time [5]. In such dense deployments, cache decisions across BSs interact non-trivially, rendering independent per-BS policies suboptimal.

Existing edge caching strategies include popularity-based placement, probabilistic caching, and coded caching [3], [6], [7]. These methods typically rely on a stationary or slowly varying popularity model and often assume a fixed mapping between users and serving BSs. More recent designs incorporate spatial correlation and cooperative placement across BSs or Fog and Cloud layers [5], [8], but still depend on hand-crafted models (e.g., Zipf popularity, fixed mobility patterns) and task-specific analytical approximations. In realistic multi-cell deployments, however, popularity is heterogeneous across user groups, time-varying, and only observable through noisy request traces. This gap motivates learning-based control that can adapt to unknown popularity and network dynamics. Learning-driven edge caching has therefore received increasing attention [2]. Supervised methods use demand prediction or collaborative filtering to infer future file popularity and then solve a deterministic placement problem [9]. Reinforcement Learning (RL) approaches treat caching as a Markov Decision Process (MDP) and learn policies that maximize cache-hit related rewards using Q-learning, policy gradients, or actor-critic methods [10]–[13]. Deep Reinforcement Learning (DRL) further integrates deep neural networks for value or policy approximation and has been widely explored for dynamic edge caching [14]–[17]. DRL-based designs can, in principle, cope with unknown and time-varying popularity and multi-cell coupling [18]. However, these systems remain tightly bound to a specific state and action parametrization and simulator, require large online interaction budgets for training, and often struggle to generalize when the network topology or traffic pattern changes drastically [19].

On the other hand, Large Language Models (LLMs) have emerged as powerful general-purpose decision makers, leveraging their inherent reasoning capabilities to operate on textual descriptions of tasks, constraints, and feedback [20]. Recent comprehensive surveys indicate that LLMs can support a wide range of telecom tasks, including configuration generation, fault diagnosis, and high-level optimization [21], [22]. In wireless networks, LLM agents have been proposed to orchestrate complex 6G functionalities [23], drive semantic communication [24], and act as radio access network (RAN) xApps for resource management [25], while LLM-enabled edge inference

frameworks optimize the placement and scheduling of LLM computation across wireless edge servers [26]. These works highlight the promise of LLMs as general decision engines that can ingest rich textual context, but they mostly use LLMs as high-level assistants, off-line solvers, or part of a hybrid pipeline, rather than as fully code-driven controllers interacting with the same environment interface used at evaluation time.

Motivated by the limitations of conventional heuristics in handling multi-cell interference and the poor generalization of DRL agents under drastic dynamics, we propose an LLM-based multi-BS edge caching framework in which the LLM is the decision maker and interacts with the environment through a strict textual interface. To effectively align the general-purpose decision maker with this rigorous control task, we employ a two-stage training paradigm consisting of Supervised Fine-Tuning (SFT) on expert demonstrations followed by Group Relative Policy Optimization (GRPO) [27] for reward-driven improvement. Our main contributions are as follows:

- This paper formalizes a unified multi-BS cooperative edge caching environment characterized by overlapping cells, heterogeneous grouped Zipf user preferences, and multi-scale frequency statistics. Crucially, this formulation does not require any parametric popularity model. The environment exposes a strict textual state and action interface, ensuring that the LLM operates under the same constraints as practical controllers.
- We develop a fully code-driven training pipeline utilizing a tailored GRPO fine-tuning scheme. We first initialize the policy via SFT to ensure the model produces valid syntax. Subsequently, we optimize an “opportunity-aware” reward that quantifies the multi-step cooperative hit rate gain relative to a NoOp baseline. This design enables the LLM to learn complex coordination strategies while strictly adhering to validity constraints.
- This study proposes a frozen-trajectory evaluation protocol to ensure fair comparison. For each traffic seed, the request process is fixed so that all methods process identical inputs under strict parsing and sanitization. This rigorous protocol eliminates randomness in request generation and allows for the precise quantification of both decision latency and policy quality.
- Experimental results demonstrate that the proposed orchestrator effectively masters cooperative logic, matching **98.9%** of the single-step exhaustive-search oracle in the standard 5-BS scenario and even slightly outperforming it in 2-BS settings (0.542 vs. 0.536). Moreover, the proposed approach exhibits robust zero-shot transferability across varying network scales and traffic statistics, highlighting its potential for flexible deployment in wireless networks without the need for frequent retraining.

II. RELATED WORK

A. Analytical and Heuristic Edge Caching

The coded caching framework [3] established fundamental gains via structured placement, while systems like Femto-Caching [4] and D2D caching [6] showed that proximity-based

storage substantially improves throughput and latency. Subsequent works extended these to fog-aided [7] and cooperative multi-cell architectures [5]. Although recent efforts incorporate temporal dynamics through freshness-aware caching [28] and online learning [29], [30], most designs rely on optimization under parametric demand assumptions, requiring relaxations for tractability. In cooperative multi-cell settings, strong spatial coupling and an exponential decision space often lead to decoupled approximations that sacrifice coordination gains.

To bridge caching decisions with wireless constraints, cross-layer optimization jointly considers communication, energy, and physical-layer mechanisms. Such formulations can optimize energy-latency trade-offs [28], [31] and integrate advanced technologies like STARS [32], but they typically yield complex mixed-integer programs. Consequently, these methods incur high computational overhead and require accurate demand models, limiting real-time deployment and adaptability to evolving constraints.

B. Learning-Based and DRL-Based Edge Caching

To cope with unknown and time-varying popularity, learning-based caching approaches leverage historical requests to infer future demand. Prediction-based methods first estimate future demand using time-series models or deep networks and then solve a deterministic placement problem [9]. While effective when predictions are accurate, this two-stage pipeline can be brittle: forecast errors directly propagate to placement decisions, and retraining is often required when the topology or serving graph changes.

Reinforcement learning instead optimizes cache updates directly from interaction data. Sadeghi *et al.* [10] and Chien *et al.* [11] applied RL and Q-learning to small-cell and collaborative caching, while Wu *et al.* [14] and Zhong *et al.* [33] leveraged deep function approximation to handle dynamic popularity and large discrete action spaces. To improve scalability in cooperative settings, Zhang *et al.* [16] incorporated federated training, and multi-agent designs have been explored for distributed coordination [34], [35]. DRL has also been used for large-scale adaptive caching and coded caching under uncertain popularity [15], [36]. While DRL offers adaptability, it suffers from poor sample efficiency and overfitting to specific topologies. A minor change in the number of users or cache size often renders a trained DRL policy invalid, necessitating computationally expensive retraining from scratch [37], and the learned policies are often tied to specific numerical state/action encodings and simulators, limiting transferability without substantial retraining.

C. LLM-Enabled Wireless Networking and Caching

LLMs are increasingly explored as general-purpose assistants and controllers in telecommunications and wireless networks, supporting tasks such as configuration synthesis, code generation, and optimization-oriented reasoning [21], [22]. Representative examples include multimodal LLM agents for 6G networking [23], LLM-enabled xApps for near-real-time RAN control [25], and LLM-driven semantic communication systems for visual transmission [24]. In parallel, edge

inference frameworks such as “Beyond the Cloud” [26] study how to partition and schedule LLM inference across wireless edge nodes to meet latency and communication constraints. These studies highlight the promise of LLMs to reason over heterogeneous context, but also underscore practical challenges in grounding outputs to strict feasibility constraints and meeting tight runtime budgets. At the networking layer, Wu *et al.* [38] further demonstrated that LLM-centric workflows can be adapted to diverse network operation tasks, and broader discussions anticipate sustained impact on automation and troubleshooting pipelines [39].

However, the intersection of LLMs and edge caching has thus far focused predominantly on *model caching*, namely optimizing the partitioning and placement of LLM parameters or intermediate states at the edge to minimize inference latency [23], [26]. In these works, the LLM is the object to be cached rather than the decision engine for conventional content placement. Using LLMs as direct, online controllers for content caching, with outputs verifiably aligned to feasibility constraints under a strict execution interface, remains relatively underexplored.

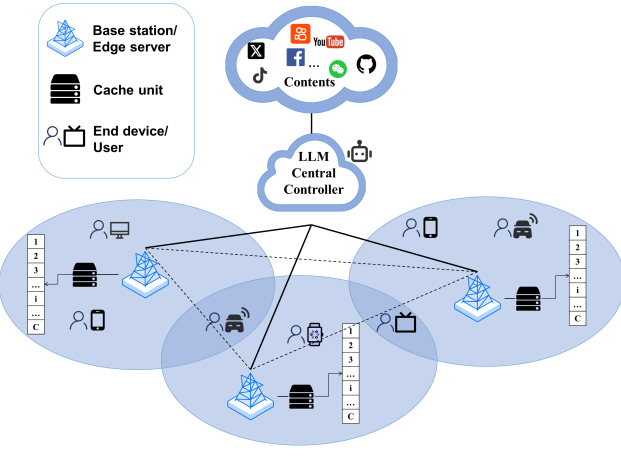


Fig. 1. Multi-cell cooperative edge caching architecture with overlapping BS coverage.

III. DECENTRALIZED EDGE CACHING IN MULTI-CELL NETWORKS: SYSTEM MODEL AND PROBLEM FORMULATION

A. System Model

We consider a cooperative multi-cell edge caching architecture as illustrated in Fig. 1. The origin server stores the full content library $\mathcal{F} = \{1, \dots, F\}$ and serves requests that miss the cache through the backhaul. At the network edge, a set of B cache-enabled Base Stations, denoted by $\mathcal{B} = \{1, \dots, B\}$, are deployed. Each BS $b \in \mathcal{B}$ is co-located with an edge server possessing a storage capacity of C_b files, where all files are assumed to have equal size. Time is slotted with index $t \in \{1, 2, \dots\}$.

Due to the dense deployment, coverage regions of BSs may overlap, meaning a user can be within the communication

range of multiple BSs simultaneously. Let $\mathcal{U}^{(t)}$ denote the set of active users at slot t , and let $\mathcal{B}_u \subseteq \mathcal{B}$ denote the set of BSs covering user u . Under this cooperative framework, a user request is considered a cache hit and served locally if the content is available in any BS within the neighborhood \mathcal{B}_u ; otherwise, it is retrieved from the origin server. We assume the user-BS association is fixed within each slot but may evolve slowly across slots due to user mobility.

a) Request Model: Each user $u \in \mathcal{U}^{(t)}$ generates one content request $f_u^{(t)} \in \mathcal{F}$ per slot. While the underlying request process is unknown to the caching controller and may exhibit temporal concept drift, it is typically modeled using heavy-tailed distributions such as the Zipf distribution [4] to capture the realistic characteristic that a small subset of popular contents dominates the aggregate demand. For each BS b , the locally observed requests at slot t constitute a multiset, as multiple users may request the same file concurrently. We capture this local request intensity by the request count $n_{b,f}^{(t)}$, defined as:

$$n_{b,f}^{(t)} \triangleq \left| \left\{ u \in \mathcal{U}^{(t)} : b \in \mathcal{B}_u, f_u^{(t)} = f \right\} \right|. \quad (1)$$

To determine candidate contents for caching, we deduplicate this multiset into an admissible insertion set $\mathcal{R}_t^{(b)}$:

$$\mathcal{R}_t^{(b)} \triangleq \{f \in \mathcal{F} : n_{b,f}^{(t)} > 0\} = \{f_u^{(t)} : u \in \mathcal{U}^{(t)}, b \in \mathcal{B}_u\}. \quad (2)$$

This set enforces a reactive caching policy where only contents requested within the current slot are eligible for insertion. Meanwhile, the count $n_{b,f}^{(t)}$ serves as an auxiliary state feature that preserves the intensity of instantaneous demand.

b) Cache State and Update Model: Let $x_{b,f}^{(t)} \in \{0, 1\}$ be a binary indicator variable where $x_{b,f}^{(t)} = 1$ implies that file f is stored at BS b during slot t . We denote the caching vector of BS b as $\mathbf{x}_b^{(t)} = (x_{b,1}^{(t)}, \dots, x_{b,F}^{(t)})$. Consequently, the global caching configuration at slot t is represented by the matrix $\mathbf{X}^{(t)} \in \{0, 1\}^{B \times F}$, formed by stacking the vectors $\{\mathbf{x}_b^{(t)}\}_{b \in \mathcal{B}}$.

To ensure practical online operation and limit backhaul bandwidth consumption during content fetching, we adopt a constrained update interface. Specifically, each BS performs at most one cache update per slot. It can either maintain the current state, denoted as `NoOp`, or perform a single-file replacement by evicting one existing file to insert one new file from the admissible set. Under this update model, the size of the local action space $D_b^{(t)}$ for BS b is given by:

$$D_b^{(t)} = C_b \cdot |\mathcal{R}_t^{(b)}| + 1. \quad (3)$$

The action space consists of the `NoOp` action plus all feasible distinct pairs of an eviction target and an insertion candidate.

B. Problem Formulation

Building on the system model, we formulate the cooperative caching control problem where BS caches are updated sequentially to maximize the long-term network-wide cache hit rate.

Optimization Constraints The caching decisions must satisfy the following constraints at every slot t :

- Storage Capacity: $\sum_{f=1}^F x_{b,f}^{(t)} \leq C_b$ for all $b \in \mathcal{B}$.

- Update Limit: The transition from $\mathbf{X}^{(t-1)}$ to $\mathbf{X}^{(t)}$ must comply with the single-replacement rule. Mathematically, this restricts the Hamming distance between consecutive states such that $\sum_{f=1}^F |x_{b,f}^{(t)} - x_{b,f}^{(t-1)}| \leq 2$ for all $b \in \mathcal{B}$.

Let $\mathbf{X} = \{\mathbf{X}^{(t)}\}_{t \geq 1}$ denote the sequence of caching decisions over time.

Performance Metric: Cooperative Hit Rate Let $\mathcal{Q}^{(t)} = \{(u, f_u^{(t)}) : u \in \mathcal{U}^{(t)}\}$ denote the set of user-request pairs at slot t . A request is considered a cache hit if the requested file is available in the cache of at least one BS covering the user. Ideally, the network scheduler directs the user to a specific serving BS $b \in \mathcal{B}_u$ that holds the content. We define the cooperative availability indicator $\mathbf{1}(u, f_u^{(t)})$ as:

$$\mathbf{1}(u, f_u^{(t)}) = \begin{cases} 1, & \text{if } \sum_{b \in \mathcal{B}_u} x_{b,f_u^{(t)}}^{(t)} \geq 1, \\ 0, & \text{otherwise.} \end{cases} \quad (4)$$

The instantaneous network cache hit rate, $P_{\text{hit}}(t)$, is calculated as the ratio of satisfied requests to the total number of active users:

$$P_{\text{hit}}(t) = \frac{1}{|\mathcal{U}^{(t)}|} \sum_{u \in \mathcal{U}^{(t)}} \mathbf{1}(u, f_u^{(t)}). \quad (5)$$

Optimization Objective We formulate the optimization problem \mathbf{P} to identify the optimal decision sequence \mathbf{X} that maximizes the long-term average cache hit rate. While real-world traffic patterns are dynamic, we define the objective under the standard stationarity and ergodicity assumption on $\{\mathcal{Q}^{(t)}\}$ so that the long-run time average exists almost surely:

$$\mathbf{P} : \underset{\mathbf{X}}{\text{maximize}} \quad \lim_{T \rightarrow \infty} \frac{1}{T} \sum_{t=1}^T P_{\text{hit}}(t) \quad (6a)$$

$$\text{subject to} \quad \sum_{f=1}^F x_{b,f}^{(t)} \leq C_b, \quad \forall b, t, \quad (6b)$$

$$\sum_{f=1}^F |x_{b,f}^{(t)} - x_{b,f}^{(t-1)}| \leq 2, \quad \forall b, t \geq 2, \quad (6c)$$

$$x_{b,f}^{(t)} \in \{0, 1\}, \quad \forall b, f, t. \quad (6d)$$

Constraint (6b) enforces storage limits, and (6d) ensures binary variables. Constraint (6c) formalizes the single-file replacement interface. Directly solving \mathbf{P} is intractable; the joint caching problem over overlapping coverage is known to be NP-hard even with known demand [4], while practical deployment is further complicated by the lack of a priori knowledge of future requests and the presence of non-stationary distribution shifts [10]. Consequently, the controller must employ a learning-based approach to adapt the policy \mathbf{X} online based on observed request streams. In the following section, we cast this sequential decision problem as a MDP and develop an executable, LLM-based policy learning framework.

IV. METHODOLOGY

This section details the proposed LLM-driven framework for cooperative multi-BS edge caching. As illustrated in Fig. 2, we formulate the problem as a MDP with a strict textual interface.

We implement a deterministic encoder-parser mechanism to instantiate the LLM as an executable policy, aligned via a two-stage training paradigm: SFT on expert trajectories followed by GRPO.

A. MDP Formulation and Executable Interface

We model the online cache update process as a sequential decision process where the agent observes the global network state and determines specific update actions for all BSs simultaneously.

a) State Space: The state s_t at slot t encapsulates the instantaneous system status and historical demand context. Formally, we define the state as the tuple:

$$s_t \triangleq \left(\mathbf{X}^{(t)}, \{\mathcal{R}_t^{(b)}\}_{b \in \mathcal{B}}, \phi^{(t)} \right), \quad (7)$$

where $\mathbf{X}^{(t)}$ represents the current global cache configuration, and $\mathcal{R}_t^{(b)}$ is the admissible insertion set for BS b derived from current requests. To capture time-varying popularity trends, $\phi^{(t)}$ denotes a collection of multi-scale request-frequency features. Let $\mathcal{W} \subset \mathbb{N}_+$ be a set of window lengths. For each file f and BS b , we compute the historical appearance rate $\phi_{b,f}^{(t)}(w)$ over window $w \in \mathcal{W}$:

$$\phi_{b,f}^{(t)}(w) \triangleq \frac{1}{\min\{w, t\}} \sum_{\tau=\max\{1, t-w+1\}}^t \mathbf{1}(f \in \mathcal{R}_\tau^{(b)}), \quad (8)$$

where $\mathbf{1}(\cdot)$ is the indicator function. By aggregating statistics over varying horizons, $\phi^{(t)}$ enables the LLM to distinguish between transient noise and stable popularity shifts.

b) Action Space and Feasibility: At each slot t , the decision for BS b , denoted by $a_{b,t}$, is either to maintain the current cache or to perform a single-file replacement. A replacement action is characterized by the tuple $(z_b, f_b^{\text{in}}, f_b^{\text{out}})$, where $z_b \in \{1, \dots, C_b\}$ is the cache slot index, f_b^{in} is the new content to insert, and f_b^{out} is the content to be evicted. The joint action is denoted by $a_t = (a_{1,t}, \dots, a_{B,t})$.

To ensure strict physical executability, we define a feasibility set function $\mathcal{A}(s_t)$. A joint action a_t is valid, i.e., $a_t \in \mathcal{A}(s_t)$, if and only if every component $a_{b,t}$ satisfies the following constraints:

- 1) **Admissibility:** The inserted content must be requested in the current slot:

$$f_b^{\text{in}} \in \mathcal{R}_t^{(b)}. \quad (9)$$

- 2) **Non-Duplication:** The content to be inserted must not already exist in the cache of BS b :

$$x_{b,f_b^{\text{in}}}^{(t)} = 0. \quad (10)$$

- 3) **Consistency:** The content targeted for eviction must explicitly match the file currently stored at the specified location. If slot z_b stores file f , then:

$$f_b^{\text{out}} = f \quad \text{s.t.} \quad x_{b,f}^{(t)} = 1. \quad (11)$$

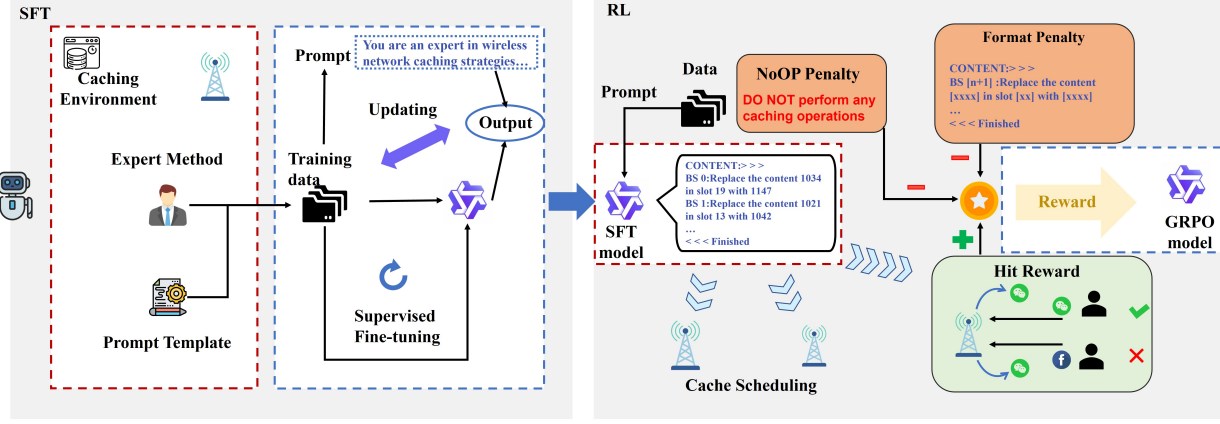


Fig. 2. Two-stage alignment pipeline. In Stage I (SFT), the LLM is trained on oracle trajectories to produce strictly executable cache-update actions. In Stage II (GRPO), the policy is fine-tuned with a shaped multi-step gain reward together with explicit format and opportunity penalties, while actions are validated and executed through the same strict parser used at deployment.

c) *Optimization Objective*: Our objective is to maximize the long-term cooperative hit rate. Since infinite-horizon optimization is intractable, we adopt the standard discounted cumulative reward formulation [40]. The objective function $J(\pi)$ for a policy π is given by:

$$\max_{\pi} J(\pi) = \mathbb{E}_{\pi} \left[\sum_{t=0}^{T-1} \gamma^t P_{\text{hit}}(t) \right], \quad (12)$$

where $\gamma \in (0, 1]$ is the discount factor that balances immediate rewards against long-term cache utility.

d) *LLM-Executable Text-to-Action Interface*: To deploy an LLM parameterized by θ as the policy π , we formalize the control loop through three deterministic transformations:

- **State-to-Prompt Encoder (\mathcal{T})**: The mapping $q_t = \mathcal{T}(s_t)$ converts the numerical state tuple—including cache content $\mathbf{X}^{(t)}$, request sets $\{\mathcal{R}_t^{(b)}\}$, and frequency features $\phi^{(t)}$ —into a structured textual prompt.
- **LLM Generation (π_{θ})**: Conditioned on prompt q_t , the model generates a textual completion $o_t \sim \pi_{\theta}(\cdot | q_t)$.
- **Text-to-Action Parser (\mathcal{P})**: The parser $\mathcal{P}(o_t)$ attempts to decode the completion into a structured action a_t . It returns a feasible action $a_t \in \mathcal{A}(s_t)$ if decoding succeeds; otherwise, we denote the output as $a_t = \text{Invalid}$ and trigger a fallback or rejection.

Consequently, the induced executable policy is defined by the composition $s_t \xrightarrow{\mathcal{T}} q_t \xrightarrow{\pi_{\theta}} o_t \xrightarrow{\mathcal{P}} a_t$.

B. Training Stage I: SFT

The primary objective of the first training stage is to bridge the gap between the open-ended generation capabilities of the LLM and the strict control interface of the caching environment. We define this code-alignment contribution as achieving two distinct goals:

- 1) **Syntax Alignment**: Ensuring the model output o_t strictly adheres to the format required by the parser \mathcal{P} , thereby minimizing syntax-based rejections.

2) **Semantic Initialization**: Imparting the fundamental logic of validity and establishing a robust baseline policy derived from expert demonstrations.

1) *Expert Data Generation*: We construct a completion-only dataset $\mathcal{D}_{\text{sft}} = \{(q_t, y_t)\}$, where $q_t = \mathcal{T}(s_t)$ is the prompt rendering of state s_t , and y_t is the target completion string. The target y_t is obtained by serializing the expert joint action $a_t^* = (a_{1,t}^*, \dots, a_{B,t}^*)$ into the requisite textual format.

To generate a_t^* , we employ a decoupled single-step exhaustive search expert. A full joint exhaustive search over all BSs is computationally intractable because the joint action space size, $|\mathcal{A}(s_t)| = \prod_{b=1}^B |\mathcal{A}_b(s_t)|$, grows exponentially with B (as formally established in Proposition 1, Appendix B), where $\mathcal{A}_b(s_t)$ denotes the feasible action set for BS b . Instead, the expert optimizes each BS b independently by enumerating all actions in $\mathcal{A}_b(s_t)$ and selecting the one that maximizes the local contribution to the cooperative hit rate over a look-ahead horizon H . While this decoupled approach ignores inter-BS coupling, it serves to align the LLM with strict action validity and provides a robust initialization for the subsequent cooperative learning stage.

The data generation process, summarized in Algorithm 1, begins with a warm-up phase of length T_w . This ensures that the cache states $\mathbf{X}^{(t)}$ and the historical frequency statistics $\phi^{(t)}$ are fully populated and representative of steady-state operation before sampling begins.

2) *Supervised Fine-Tuning*: We fine-tune the model parameter θ using QLoRA [41] with a rank of $r=64$. The training objective is to maximize the likelihood of generating the expert decision string y_t given the state prompt q_t . Let $y_t = (y_{t,1}, y_{t,2}, \dots, y_{t,L_t})$ be the token sequence of length L_t corresponding to the target completion. The loss function $\mathcal{L}_{\text{sft}}(\theta)$ is defined as the standard causal language modeling loss:

$$\mathcal{L}_{\text{sft}}(\theta) = -\mathbb{E}_{(q,y) \sim \mathcal{D}_{\text{sft}}} \left[\sum_{n=1}^{L_t} \log \pi_{\theta}(y_n | q, y_{<n}) \right], \quad (13)$$

Algorithm 1 Stage I: SFT Data Generation and Training

Require: Environment \mathcal{E} ; encoder \mathcal{T} ; horizon H ; warmup T_w ; target size N

- 1: Initialize dataset $\mathcal{D}_{\text{sft}} \leftarrow \emptyset$
- 2: Reset \mathcal{E} and run expert policy for T_w steps (warm-up)
- 3: **while** $|\mathcal{D}_{\text{sft}}| < N$ **do**
- 4: Observe state s_t ; compute request sets $\{\mathcal{R}_t^{(b)}\}$
- 5: **for** $b = 1$ to B **do**
- 6: $a_{b,t}^* \leftarrow \text{LOOKAHEADORACLE}(\mathcal{E}, b, \mathcal{R}_t^{(b)}, H)$
- 7: **end for**
- 8: **if** all BS caches are full **then**
- 9: $q_t \leftarrow \mathcal{T}(s_t)$
- 10: $y_t \leftarrow \text{Serialize}(\{a_{b,t}^*\}_{b=1}^B)$ \triangleright Convert actions to text
- 11: $\mathcal{D}_{\text{sft}} \leftarrow \mathcal{D}_{\text{sft}} \cup \{(q_t, y_t)\}$
- 12: **end if**
- 13: Step \mathcal{E} using joint action $\{a_{b,t}^*\}_{b=1}^B$
- 14: **end while**
- 15: Train π_θ on \mathcal{D}_{sft} by minimizing Eq. (13)
- 16: **return** SFT model $\pi_{\theta_{\text{sft}}}$

where $y_{<n}$ denotes the prefix of the target sequence. To concentrate the model on the non-trivial replacement logic, we selectively collect SFT samples only when all BS caches are full, as this regime requires the agent to make complex eviction decisions rather than simple insertions. Throughout SFT, we keep the state encoder $\mathcal{T}(\cdot)$ and the strict parser $\mathcal{P}(\cdot)$ fixed. This ensures that the training process directly optimizes the exact executable interface used during deployment.

C. Training Stage II: GRPO Fine-Tuning

While SFT establishes valid action syntax and initializes the policy, it relies on a decoupled approximation that ignores inter-BS correlations and lacks exploration. To transcend these limits, we employ GRPO to strictly optimize the cooperative objective. We select GRPO specifically because our reward structure measures fine-grained marginal gains over a `NoOp` baseline; unlike value-based critics that struggle to estimate such subtle differences, GRPO’s group normalization amplifies relative improvements, ensuring robust gradient signals without the complexity and instability of training a separate value network.

1) *Opportunity-Aware Reward Design*: The core of the RL stage is a reward mechanism that assigns credit to actions yielding deferred cooperative benefits while enforcing strict constraints. We construct a composite reward signal $R(o_t)$ based on the delta-weighted cooperative gain.

First, we define the look-ahead value function. Let \mathbf{X} denote a generic global cache configuration. We generalize the instantaneous hit rate to $P_{\text{hit}}(\mathbf{X}, \mathcal{Q})$, representing the hit rate of configuration \mathbf{X} under request set \mathcal{Q} . Under the frozen-trajectory protocol, let $\mathcal{Q}^{(t+1:t+H)} \triangleq (\mathcal{Q}^{(t+1)}, \dots, \mathcal{Q}^{(t+H)})$ denote the fixed sequence of future requests. The normalized discounted look-ahead value \mathcal{H}_H is defined as:

$$\mathcal{H}_H(\mathbf{X}; \mathcal{Q}^{(t+1:t+H)}) \triangleq \frac{\sum_{k=1}^H \gamma^{k-1} P_{\text{hit}}(\mathbf{X}, \mathcal{Q}^{(t+k)})}{\sum_{k=1}^H \gamma^{k-1}}. \quad (14)$$

In our implementation, this oracle evaluator is realized by directly querying the frozen future request trace during the training phase, providing a computationally efficient and low-variance ground-truth signal for policy optimization.

Next, we quantify the marginal improvement generated by the model’s output. At slot t , let o_t be the textual completion generated by the policy, and let $a_t \triangleq \mathcal{P}(o_t)$ denote the parsed joint action, where $a_t = \text{Invalid}$ indicates a non-executable output. If a_t is valid, the environment transitions from the current state $\mathbf{X}^{(t)}$ to a new state $\mathbf{X}^{(t+1)}$ according to the update rule: $\mathbf{X}^{(t+1)} = \text{Update}(\mathbf{X}^{(t)}, a_t)$. The delta-weighted gain, $\Delta_{\text{perf}}(a_t)$, is the difference in future potential between the post-action state and the current state:

$$\Delta_{\text{perf}}(a_t) = \mathcal{H}_H(\mathbf{X}^{(t+1)}; \mathcal{Q}^{(t+1:t+H)}) - \mathcal{H}_H(\mathbf{X}^{(t)}; \mathcal{Q}^{(t+1:t+H)}). \quad (15)$$

This differential formulation acts as a baseline subtraction, ensuring that rewards reflect the quality of the decision rather than the intrinsic request intensity of the time slot.

To strictly enforce the interface and suppress suboptimal passivity, we define a penalty function $\Psi(o_t)$:

$$\Psi(o_t) = \begin{cases} \lambda_{\text{fmt}}, & \text{if } a_t = \text{Invalid} \text{ (format error),} \\ \lambda_{\text{opp}}, & \text{if } a_t = \text{NoOp} \text{ and } a_t^* \neq \text{NoOp}, \\ 0, & \text{otherwise.} \end{cases} \quad (16)$$

where $\lambda_{\text{fmt}} < 0$ is a static formatting penalty, and $\lambda_{\text{opp}} < 0$ is a dynamic opportunity penalty. Here, a_t^* is the expert joint action defined in Section IV-B; we use the condition $a_t^* \neq \text{NoOp}$ as a training-time witness that a beneficial replacement exists, avoiding explicit counterfactual enumeration (see Section IV-D). This selectively discourages passivity without altering the preference ordering among valid active updates. For invalid outputs, no cache update is executed, and we set $\Delta_{\text{perf}}(a_t) = 0$.

The final scalar reward $R(o_t)$ is the clipped sum of the gain and the penalty:

$$R(o_t) = \text{clip}(\Delta_{\text{perf}}(a_t) + \Psi(o_t), -1, 1). \quad (17)$$

2) *GRPO Objective*: We optimize the policy π_θ using GRPO, which eliminates the need for a separate value network critic. For each state prompt q_t , the policy samples a group of M independent completions $\{o_{t,i}\}_{i=1}^M$. To reduce variance caused by non-stationary traffic patterns, we compute the group-relative Advantage A_i by standardizing the rewards within the sampled group:

$$A_i = \frac{R(o_{t,i}) - \mu_{\mathbf{R}}}{\sigma_{\mathbf{R}} + \epsilon}, \quad (18)$$

where $\mu_{\mathbf{R}}$ and $\sigma_{\mathbf{R}}$ are the mean and standard deviation of the reward set $\mathbf{R} = \{R(o_{t,j})\}_{j=1}^M$, and ϵ is a small stability constant.

The policy parameters θ are updated by maximizing the following surrogate objective, which incorporates a proximal policy optimization-style clipping mechanism [42] and a

Kullback-Leibler (KL) divergence constraint to prevent deviation from the SFT initialization π_{ref} :

$$\mathcal{J}_{\text{GRPO}}(\theta) = \mathbb{E}_{q_t \sim \mathcal{D}} \left[\frac{1}{M} \sum_{i=1}^M \min \left(\rho_i(\theta) A_i, \text{clip}(\rho_i(\theta), 1 - \varepsilon, 1 + \varepsilon) A_i \right) - \beta D_{\text{KL}}(\pi_\theta(\cdot | q_t) \| \pi_{\text{ref}}(\cdot | q_t)) \right], \quad (19)$$

where $\rho_i(\theta) = \frac{\pi_\theta(o_{t,i} | q_t)}{\pi_{\text{ref}}(o_{t,i} | q_t)}$ is the importance sampling ratio, ε is the clipping range, and β controls the strength of the KL regularization.

D. Reward Architecture Analysis

This subsection analyzes the reward design from two perspectives: (i) the efficient implementation of the opportunity-aware penalty, and (ii) its interpretation as Potential-Based Reward Shaping (PBRS) [43] to preserve policy optimality.

1) *Efficient Opportunity-Aware Penalty*: A key challenge is distinguishing intentional inaction (NoOp) from missed improvements. Directly implementing the condition in Eq. (16) would require enumerating counterfactual write actions to verify if a gain-positive replacement exists, which is computationally prohibitive.

We avoid this by leveraging the supervised data pipeline: the GRPO stage utilizes training states where a reference action a_t^* is available from the oracle trajectory (Section IV-B). Let a_t denote the parsed joint action from the model completion. We define the opportunity penalty $P_t(a_t)$ as:

$$P_t(a_t) = \begin{cases} \lambda_{\text{opp}}, & \text{if } a_t = \text{NoOp and } a_t^* \neq \text{NoOp} \\ 0, & \text{otherwise} \end{cases} \quad (20)$$

where $\lambda_{\text{opp}} < 0$. Here, $a_t^* \neq \text{NoOp}$ serves as a training-time *witness* that a beneficial update exists, avoiding runtime enumeration of the action space. This targeted demotion only penalizes NoOp when the reference policy identifies a gain-positive replacement, ensuring the relative ordering of valid write actions remains unaffected (Theorem 1).

2) *Theoretical Analysis and PBRS Guarantees*: We now connect the proposed reward to PBRS theory. Under the frozen-trajectory protocol, the multi-step gain in Eq. (15) can be viewed as a potential-difference shaping term [43], which preserves the optimal policy. The opportunity penalty then acts purely as a correction against degenerate passivity.

Ignoring the clipping operation in Eq. (17) and the formatting penalty that exclusively affects non-executable outputs, we define the unclipped per-slot shaped reward as:

$$\tilde{R}_t(a_t) = \Delta_{\text{perf}}(a_t) + P_t(a_t). \quad (21)$$

Under the frozen-trajectory look-ahead protocol, we view the environment as having an augmented state $\bar{s}^{(t)} \triangleq (s_t, \mathcal{Q}^{(t+1:t+H)})$, i.e., appending the next H request sets to the observable state.

Theorem 1 (PBRS Invariance and Opportunity Correction). *Define the state potential function as $\Phi(\bar{s}^{(t)}) \triangleq \mathcal{H}_H(\mathbf{X}^{(t)}, \mathcal{Q}^{(t+1:t+H)})$. The reward structure satisfies:*

- 1) **Decision Invariance**: The performance gain Δ_{perf} constitutes a potential-difference signal. Maximizing the shaped reward is mathematically equivalent to maximizing the post-action potential:

$$\begin{aligned} & \arg \max_{a_t} \Delta_{\text{perf}}(a_t) \\ &= \arg \max_{a_t} \left[\Phi(\bar{s}^{(t+1)}(a_t)) - \Phi(\bar{s}^{(t)}) \right] \\ &= \arg \max_{a_t} \Phi(\bar{s}^{(t+1)}(a_t)). \end{aligned} \quad (22)$$

- 2) **Order Preservation & Strict Demotion**: The penalty P_t preserves the relative ranking among write actions while strictly demoting NoOp whenever it is dominated. For any write action w :

$$\Delta_{\text{perf}}(w) > \Delta_{\text{perf}}(\text{NoOp}) \implies \tilde{R}_t(w) > \tilde{R}_t(\text{NoOp}).$$

The proof of Theorem 1 is provided in Appendix A. This analysis demonstrates that the proposed reward structure serves a dual purpose: the potential function reduces variance to facilitate stable convergence, while the invariance property theoretically guarantees that the final LLM controller is optimized for the true system objective, namely the cooperative edge caching efficiency.

V. SIMULATION EXPERIMENTS AND RESULT ANALYSIS

We evaluate the proposed framework under a frozen-trajectory protocol for reproducibility and paired comparison. For each seed, we generate a task instance consisting of (i) a user-BS association graph induced by a geometric overlap model and (ii) a multi-user request trace, and then reuse the same instance across all methods. This eliminates performance variance caused by stochastic topology realizations and isolates decision quality under the same strict single-swap interface.

A. Experimental Setup

1) *Simulation Environment and Traffic Model*: We simulate the slotted cache-update process described in Section III. We consider two network scales: a two-BS setting for ablations and a five-BS setting for scalable coordination. In each instance, BS locations are fixed on a simple layout, while user locations are sampled uniformly over the service area; each user is connected to all BSs within a coverage radius, yielding overlapping neighborhoods and non-trivial cooperative coupling.

User requests follow a grouped-Zipf model: each group draws a distinct, randomly permuted Zipf ranking over the library and users inherit their group's distribution. This construction creates heterogeneous and spatially non-uniform popularity, different BSs observe different mixtures of user groups, while retaining the heavy-tailed demand patterns commonly assumed in edge caching.

To avoid cold-start artifacts and ensure stable historical statistics, we warm-start each frozen instance by running a fixed expert prefill policy for 100 slots to populate caches and history buffers. All controllers are then evaluated from the same warm-started state under the same frozen requests and association graph.

TABLE I
DEFAULT SIMULATION PARAMETERS (UNLESS EXPLICITLY SWEEPED).

Parameter	Value
BSs B	2, 5
Users U	20 (two-BS), 40 (five-BS)
Library size F	100 (unless swept)
Cache size C_b	10 (all b , unless swept)
Groups G	3
Zipf skew α	1.2 (unless swept)
History windows \mathcal{W}	$\{10, 100, 1000\}$ slots
Evaluation decoding	greedy ($T=0$)

2) *Implementation Details*: We instantiate the controller with **Qwen2.5-7B-Instruct** [44] and fine-tune it via QLoRA to keep the backbone fixed while adapting to the strict prompt, action interface. For evaluation, we use greedy decoding together with the same parser as in training to remove generation randomness and ensure strict executability. Default parameters are summarized in Table I; unless explicitly swept, we use $\mathcal{W} = \{10, 100, 1000\}$ to expose short, medium, long-term demand signals.

3) *Baselines*: We benchmark against representative reactive eviction heuristics and a DRL baseline. All methods operate under the same admissible insertion sets $\mathcal{R}_t^{(b)}$ and the same single-swap update constraint; the LLM-based controller additionally uses strict parsing and feasibility verification to guarantee executability.

- **Least Recently Used (LRU)** [45]: This policy evicts the least recently requested cached content.
- **Least Frequently Used (LFU)** [46]: This strategy evicts the least frequently requested content based on accumulated counts, although it remains vulnerable to cache pollution under non-stationary demand.
- **First-In First-Out (FIFO)** [47]: This method evicts the oldest cached content based strictly on insertion order.
- **Soft Actor-Critic (SAC)** [48]: We employ SAC as a maximum-entropy DRL baseline, trained with a numerical state/action encoding under the same constrained action interface.
- **Single-step Exhaustive Search**: This myopic reference enumerates NoOp and all feasible single-slot replacements for each BS to maximize the immediate cooperative hit rate. While its per-slot cost scales as $\mathcal{O}(C_b|\mathcal{R}_t^{(b)}|)$, extending it to full joint enumeration across BSs is infeasible due to the exponential growth of the joint action space (see Appendix B).

B. Reward Design Validation

Before conducting the full benchmark, we validate the GRPO reward design to ensure stable optimization. Directly optimizing the raw cooperative hit rate can induce high-variance updates, as the absolute metric fluctuates substantially with request diversity and overlap patterns, obscuring the true quality of decisions. We therefore adopt a baseline-subtracted reward that measures the relative improvement over

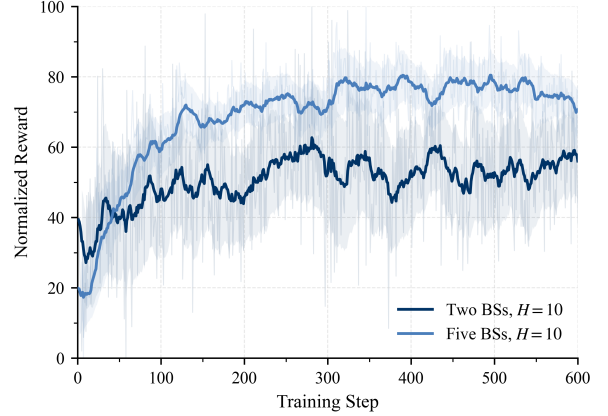


Fig. 3. Representative GRPO training trajectories under strict executability (normalized reward vs. training step) for two-BS and five-BS settings.

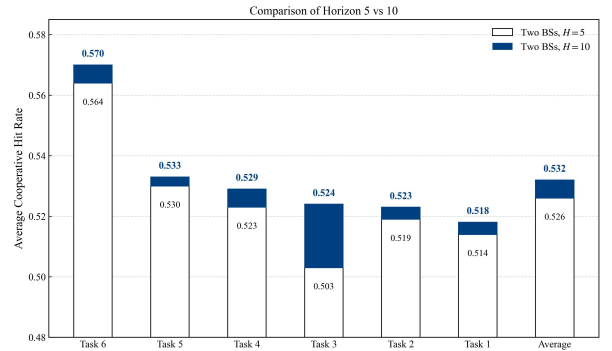


Fig. 4. Two-BS horizon comparison across three frozen tasks: training with $H=10$ consistently improves cooperative hit rate over $H=5$.

a NoOp baseline under the same cache and request state. As illustrated in Fig. 3, this normalized signal enables the training curves to rise steadily and plateau without oscillation in both two-BS and five-BS settings, confirming that the constrained text-to-action policy is reliably learnable. Furthermore, we investigate the impact of the look-ahead horizon H . As shown in Fig. 4, extending the horizon from $H=5$ to $H=10$ consistently improves the cooperative hit rate. A longer horizon captures delayed benefits, such as reduced redundancy across overlapping BSs, that are invisible to shorter-term feedback. Consequently, all subsequent experiments utilize the baseline-subtracted reward with $H=10$.

C. Performance Evaluation

We report results on three frozen instances (seeds) per scenario, where both the request trace and the user-BS association graph are fixed as described in Section V-A. After warm-starting, each controller is rolled out for $T=300$ decision slots under the strict single-swap constraint. To summarize both early adaptation and steady-state stability, we report the prefix-average cooperative hit rate, $\bar{P}_{\text{hit}}(t) \triangleq \frac{1}{t} \sum_{\tau=1}^t P_{\text{hit}}(\tau)$, at $t \in \{50, 100, \dots, 300\}$ and the overall mean.

a) *Two-BS Scenario*: Table II confirms that GRPO consistently outperforms SFT and all baselines throughout the

TABLE II

TWO-BS PERFORMANCE ON THREE FROZEN SEEDS. PREFIX AVERAGES AT SLOTS $\{50, 100, \dots, 300\}$ AND OVERALL MEAN. THE **BOLD** AND UNDERLINED VALUES REPRESENT THE BEST AND SECOND-BEST PERFORMANCE, RESPECTIVELY.

Method	Average Cooperative Hit Rate (\uparrow)						
	Slot 50	Slot 100	Slot 150	Slot 200	Slot 250	Slot 300	Mean
GRPO LLM	0.530	0.536	0.538	0.545	0.550	0.552	0.542
SFT LLM	0.522	0.526	0.525	0.534	0.538	0.540	0.531
Exhaustive	<u>0.526</u>	<u>0.531</u>	<u>0.536</u>	<u>0.540</u>	<u>0.543</u>	<u>0.541</u>	<u>0.536</u>
SAC	0.462	0.474	0.477	0.481	0.482	0.482	0.477
LRU	0.491	0.499	0.503	0.507	0.508	0.507	0.502
LFU	0.471	0.494	0.498	0.503	0.506	0.507	0.497
FIFO	0.318	0.312	0.308	0.317	0.314	0.309	0.313

rollout. Remarkably, GRPO slightly exceeds even the single-step exhaustive reference. This advantage stems from a fundamental objective mismatch: while the exhaustive policy myopically maximizes the immediate hit rate, GRPO is trained on a multi-step gain. This training signal enables the agent to make strategic replacements that, while locally suboptimal in the current slot, effectively reduce future content redundancy across overlapping coverage zones. In contrast, heuristic rules like LRU and LFU perform poorly because they rely solely on local recency or frequency signals. Lacking mechanisms to reason about network-level complementarity, they often replicate popular content across neighboring BSs, wasting aggregate storage capacity. Finally, SAC underperforms because it must explore a large, discrete, and feasibility-constrained action space from scratch. Without the structural priors provided by SFT and the stable, normalized signals inherent to GRPO, it struggles to converge using high-variance absolute rewards.

b) Five-BS Scenario: In the five-BS scenario, the coordination complexity intensifies significantly due to intricate spatial coupling and the exponential expansion of the joint action space. Despite these challenges, the GRPO-tuned framework demonstrates robust scalability, achieving a mean cooperative hit rate of **0.610**. This performance is near-optimal, matching **98.9%** of the Single-step Exhaustive Search oracle (0.617). Crucially, while the oracle relies on computationally prohibitive online enumeration to maximize immediate returns, our LLM-based controller functions as an efficient proxy solver, inferring high-quality decisions directly from the prompt without the overhead of iterative search. The method establishes a substantial margin over both the SFT initialization (0.589) and the best heuristic, LFU (0.586). Conversely, the DRL baseline (SAC) fails to scale effectively, yielding a hit rate of only 0.554. This consistent underperformance, which mirrors the results in the two-BS setting, reinforces the critical advantage of our two-stage alignment. Unlike standard DRL which struggles in high-dimensional spaces with absolute rewards, our framework successfully leverages SFT priors and the variance-reduced advantage of GRPO to master complex coordination.

D. Generalization and Robustness Tests

We assess the zero-shot generalization of a single trained controller under varying cache capacities, library sizes, de-

mand skewness, and user scales. SAC is omitted from these robustness checks due to its lack of competitiveness in the primary evaluation. To ensure that performance variations strictly reflect generalization capability rather than additional learning or relaxed executability, all sweeps adhere to a frozen trajectory protocol with identical steady-state initialization and strict action verification.

1) Two-BS zero-shot generalization: We begin with a two-BS capacity sweep, since changing C_b affects both prompt length and the admissible action space. We evaluate transfer from the training capacity $C_b=10$ to $C_b \in \{10, 15, 20, 25, 30\}$ without retraining. As shown in Table IV, GRPO generalizes robustly across the full range without retraining, despite the change in both cache-state dimensionality and feasible single-swap actions. The advantage is most pronounced at small capacities, where storage pressure is highest and each replacement decision has a large opportunity cost: a myopic eviction can permanently displace a moderately popular content that would be repeatedly requested in the near future. As C_b increases, all methods improve and the gap to exhaustive search naturally narrows, because a larger cache reduces the need for frequent evictions and makes performance less sensitive to fine-grained replacement choices.

2) Five-BS robustness sweeps: We next stress-test robustness in the more realistic five-BS cooperative setting. Here, generalization is not only about prompt length, but also about whether the learned policy remains effective under different levels of (i) storage pressure (C_b), (ii) content diversity (F), (iii) demand concentration (α), and (iv) request load and diversity (U). Each of these modifies the environment dynamics and the admissible replacement set in a different way, therefore jointly probing whether the policy has learned reusable coordination principles.

To evaluate the robustness of the proposed method, we perform a comprehensive parameter sweep without retraining the model, while strictly adhering to the frozen-trajectory protocol and ensuring strict executability. The specific ranges for the parameters C_b , F , α , and U are summarized in Table V.

a) Cache capacity C_b : Fig. 5 varies C_b . As C_b increases, the average cooperative hit rate improves for all methods due to reduced eviction pressure. Across the sweep, GRPO consistently outperforms SFT and the classical heuristics, and its margin over LFU/LRU is most visible at small-to-moderate

TABLE III
FIVE-BS PERFORMANCE ON THREE FROZEN SEEDS. PREFIX AVERAGES AT SLOTS $\{50, 100, \dots, 300\}$ AND OVERALL MEAN. THE **BOLD** AND UNDERLINED VALUES REPRESENT THE BEST AND SECOND-BEST PERFORMANCE, RESPECTIVELY.

Method	Average Cooperative Hit Rate (\uparrow)						
	Slot 50	Slot 100	Slot 150	Slot 200	Slot 250	Slot 300	Mean
GRPO LLM	<u>0.615</u>	<u>0.615</u>	<u>0.609</u>	<u>0.607</u>	<u>0.606</u>	<u>0.607</u>	<u>0.610</u>
SFT LLM	0.595	0.595	0.587	0.588	0.584	0.584	0.589
Exhaustive	0.626	0.617	0.616	0.614	0.616	0.612	0.617
SAC	0.561	0.554	0.552	0.551	0.550	0.556	0.554
LFU	0.597	0.591	0.586	0.584	0.579	0.580	0.586
LRU	0.582	0.579	0.577	0.571	0.567	0.566	0.574
FIFO	0.363	0.369	0.378	0.375	0.368	0.366	0.370

TABLE IV
TWO-BS ZERO-SHOT GENERALIZATION ACROSS CACHE CAPACITIES.
BEST PER ROW IS BOLDED.

Cache C_b	Heuristics			LLM / Reference		
	FIFO	LRU	LFU	Exhaustive	SFT	GRPO
10	0.289	0.488	0.501	0.521	0.531	0.544
15	0.371	0.589	0.598	0.616	0.612	0.624
20	0.440	0.669	0.674	0.681	0.675	0.683
25	0.501	0.729	0.728	0.739	0.731	0.734
30	0.555	0.771	0.771	0.775	0.764	0.770

TABLE V
SUMMARY OF PARAMETER SWEEP RANGES

Parameter	Search Range / Values
Cache capacity (C_b)	$\{10, 15, 20, 25, 30\}$
Library size (F)	$\{100, 300, 500, 700, 900, 1100\}$
Zipf skew (α)	$\{0.6, 0.8, 1.0, 1.2, 1.4, 1.6\}$
Users (U)	$\{20, 40, 60, 80, 100\}$

capacities (e.g., $C_b=10\text{--}20$), where storage is scarce and redundant replication across overlapping BSs is most costly. In the mid-capacity regime ($C_b=15\text{--}25$), GRPO is highly competitive with the exhaustive reference, indicating that the learned coordination can effectively diversify placements while still keeping necessary replication for frequently requested head contents. When C_b becomes large (e.g., $C_b=30$), all methods converge because most high-demand contents can be retained simultaneously, so the gap between GRPO and simple heuristics naturally shrinks.

b) *Library size F* : Fig. 6 increases F . This sweep probes robustness to content diversity and sparse reuse. As F grows, the cache-to-library ratio shrinks and repeated requests become less frequent, so all methods degrade substantially (from around 0.60 at $F=100$ to around 0.44–0.45 at $F=1100$). In this regime, purely frequency/recency based rules can be brittle: LFU can accumulate stale counts and over-retain transiently popular contents, while LRU can overreact to one-off requests and induce churn. GRPO degrades more grace-

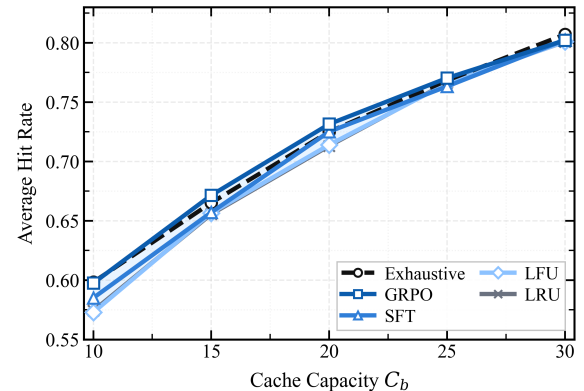


Fig. 5. Five-BS robustness sweep: cooperative hit rate vs. cache capacity C_b (zero-shot, no retraining).

fully and remains the strongest among the learned/heuristic baselines across the sweep, reflecting that the look-ahead training objective encourages replacements that improve future cooperative hits instead of reacting myopically to noisy single-slot evidence. We also observe small crossings between GRPO and the exhaustive reference at the largest F , which are consistent with finite-horizon evaluation noise; overall, GRPO tracks the strongest reference closely while maintaining clear gains over SFT/LFU/LRU.

c) *Zipf skew α* : Fig. 7 varies α , controlling demand concentration. As α increases, demand becomes more concentrated on the head, so all methods improve substantially. When the distribution is flatter-to-moderate (small α , e.g., 0.6–1.0), the long tail contributes significantly and cooperative coordination across overlapping BSs becomes essential; in this regime, GRPO maintains a consistent advantage over SFT and both heuristics by learning coverage-oriented placements under limited cache budgets. As α becomes large, caching the head dominates performance and simple heuristics become stronger, so the advantage of sophisticated coordination diminishes and the curves move closer. We further note that around $\alpha=1.4$ GRPO can match or slightly exceed the exhaustive reference in our traces, while for very concentrated demand (e.g., $\alpha=1.6$) the exhaustive reference remains highest and all methods are close due to the dominance of head contents.

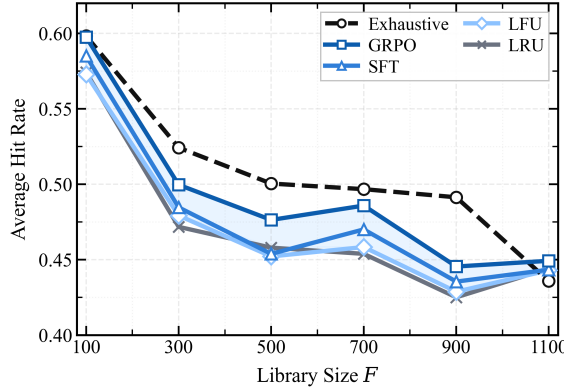


Fig. 6. Five-BS robustness sweep: cooperative hit rate vs. library size F (zero-shot, no retraining).

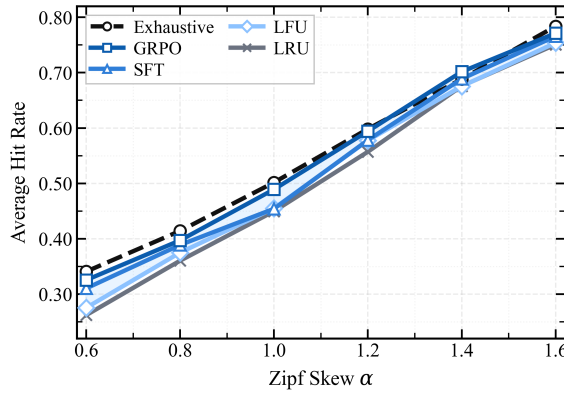


Fig. 7. Five-BS robustness sweep: cooperative hit rate vs. Zipf skew α (zero-shot, no retraining).

d) Number of Users U : Fig. 8 varies the number of users U , which changes both the per-slot request volume and the diversity of the admissible insertion pools $\{\mathcal{R}_t^{(b)}\}$. This introduces competing effects: a larger population provides richer statistical evidence to identify truly popular content, but simultaneously increases the instantaneous diversity of requests, heightening the risk of cache pollution. We observe that the Single-step Exhaustive search performs robustly at lower user densities ($U \leq 40$) but begins to degrade or stagnate as the population grows. In contrast, GRPO exhibits superior scalability, overtaking the Exhaustive baseline at $U = 60$ and achieving its peak performance at $U = 80$. This result highlights a critical advantage of the proposed method: in high-density regimes where $\mathcal{R}_t^{(b)}$ is large and noisy, the myopic Exhaustive search tends to "chase" transient requests, leading to suboptimal replacements. Conversely, GRPO's multi-step look-ahead training effectively filters this noise, prioritizing content with sustained cooperative utility over immediate but transient gains. Meanwhile, classical heuristics and SFT generally yield lower hit rates, confirming the necessity of reward-driven alignment for complex coordination.

e) Summary: Across both system scales and all zero-shot robustness sweeps, GRPO maintains robust improvements over SFT and classical eviction heuristics under strict executability.

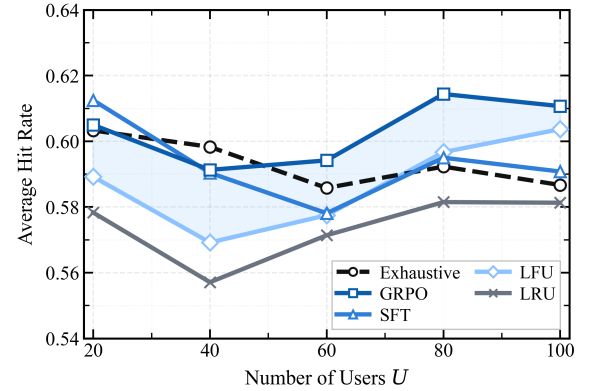


Fig. 8. Five-BS robustness sweep: cooperative hit rate vs. number of users U (zero-shot, no retraining).

Notably, the relative gains are most pronounced in the hardest regimes (small C_b , large F , and flatter popularity), where myopic local rules are most likely to waste capacity through redundant caching or cache pollution and where multi-step cooperative credit assignment is most valuable. The two-BS capacity transfer confirms that the learned policy generalizes even when the prompt structure and action space change substantially, while the five-BS sweeps demonstrate robustness to storage pressure, library diversity, demand skew, and user-driven request dynamics.

VI. CONCLUSION

In this paper, we investigated the problem of cooperative edge caching in multi-cell wireless networks by LLM as the autonomous control agent. We formulated the cache replacement task as a strictly constrained text-generation problem and proposed a two-stage alignment strategy combining SFT with GRPO to enforce feasibility and maximize long-term cooperative gains. We showed that the proposed framework effectively masters complex coordination logic without explicit modeling of the demand distribution. Numerical results under a rigorous frozen-trajectory protocol demonstrate that the learned policy achieves near-optimal performance, matching 98.9% of the exhaustive search oracle in standard scenarios and consistently outperforming classical heuristics. Furthermore, we provided experimental evidence of the controller's zero-shot transferability, showing robust performance retention across varying cache capacities, library sizes, and user densities. Future work includes extending the framework to handle variable-sized content and incorporating inference latency constraints.

REFERENCES

- [1] U. Cisco, "Cisco annual internet report (2018–2023) white paper," *Cisco: San Jose, CA, USA*, vol. 10, no. 1, pp. 1–35, 2020.
- [2] H. Li, M. Sun, F. Xia, X. Xu, and M. Bilal, "A survey of edge caching: Key issues and challenges," *Tsinghua Science and Technology*, vol. 29, no. 3, pp. 818–842, 2023.
- [3] M. A. Maddah-Ali and U. Niesen, "Fundamental limits of caching," *IEEE Transactions on Information Theory*, vol. 60, no. 5, pp. 2856–2867, 2014.

[4] K. Shanmugam, N. Golrezaei, A. G. Dimakis, A. F. Molisch, and G. Caire, "Femtocaching: Wireless content delivery through distributed caching helpers," *IEEE Transactions on Information Theory*, vol. 59, no. 12, pp. 8402–8413, 2013.

[5] S. Zhang, P. He, K. Suto, P. Yang, L. Zhao, and X. Shen, "Cooperative edge caching in user-centric clustered mobile networks," *IEEE Transactions on Mobile Computing*, vol. 17, no. 8, pp. 1791–1805, 2018.

[6] X. Li, X. Wang, P.-J. Wan, Z. Han, and V. C. Leung, "Hierarchical edge caching in device-to-device aided mobile networks: Modeling, optimization, and design," *IEEE Journal on Selected Areas in Communications*, vol. 36, no. 8, pp. 1768–1785, 2018.

[7] S. M. Azimi, O. Simeone, A. Sengupta, and R. Tandon, "Online edge caching and wireless delivery in fog-aided networks with dynamic content popularity," *IEEE Journal on Selected Areas in Communications*, vol. 36, no. 6, pp. 1189–1202, 2018.

[8] Y. Jiang, H. Feng, F.-C. Zheng, D. Niyato, and X. You, "Deep learning-based edge caching in fog radio access networks," *IEEE Transactions on Wireless Communications*, vol. 19, no. 12, pp. 8442–8454, 2020.

[9] P. Zhang, M. Sun, Y. Tu, X. Li, Z. Yang, and R. Wang, "Device–edge collaborative differentiated data caching strategy toward aiot," *IEEE Internet of Things Journal*, vol. 10, no. 13, pp. 11 316–11 325, 2023.

[10] A. Sadeghi, F. Sheikholeslami, and G. B. Giannakis, "Optimal and scalable caching for 5g using reinforcement learning of space-time popularities," *IEEE Journal of Selected Topics in Signal Processing*, vol. 12, no. 1, pp. 180–190, 2017.

[11] W.-C. Chien, H.-Y. Weng, and C.-F. Lai, "Q-learning based collaborative cache allocation in mobile edge computing," *Future generation computer systems*, vol. 102, pp. 603–610, 2020.

[12] Z. Yang, Y. Liu *et al.*, "Cache-aided noma mobile edge computing: A reinforcement learning approach," *IEEE Transactions on Wireless Communications*, vol. 19, no. 10, pp. 6899–6915, 2020.

[13] N. Yang, S. Chen, H. Zhang, and R. Berry, "Beyond the edge: An advanced exploration of reinforcement learning for mobile edge computing, its applications, and future research trajectories," *IEEE Communications Surveys & Tutorials*, vol. 27, no. 1, pp. 546–594, 2024.

[14] P. Wu, J. Li, L. Shi, M. Ding, K. Cai, and F. Yang, "Dynamic content update for wireless edge caching via deep reinforcement learning," *IEEE Communications Letters*, vol. 23, no. 10, pp. 1773–1777, 2019.

[15] T. Wang, Y. Deng, J. Mao, M. Chen *et al.*, "Towards intelligent adaptive edge caching using deep reinforcement learning," *IEEE Transactions on Mobile Computing*, vol. 23, no. 10, pp. 9289–9303, 2024.

[16] M. Zhang, Y. Jiang, F.-C. Zheng, D. Wang, M. Bennis, A. Jamalipour, and X. You, "Communication-efficient federated deep reinforcement learning based cooperative edge caching in fog radio access networks," *IEEE Transactions on Wireless Communications*, 2024.

[17] Z. Wei, Y. Zhao, Z. Lyu, X. Yuan, Y. Zhang, and L. Feng, "Cooperative caching algorithm for mobile edge networks based on multi-agent meta reinforcement learning," *Computer Networks*, vol. 242, p. 110247, 2024.

[18] C. Zhong, M. C. Gursoy *et al.*, "Deep reinforcement learning-based edge caching in wireless networks," *IEEE Transactions on Cognitive Communications and Networking*, vol. 6, no. 1, pp. 48–61, 2020.

[19] K. Rusek, J. Suárez-Varela, P. Almasan, P. Barlet-Ros, and A. Cabellos-Aparicio, "Routenet: Leveraging graph neural networks for network modeling and optimization in sdn," *IEEE Journal on Selected Areas in Communications*, vol. 38, no. 10, pp. 2260–2270, 2020.

[20] S. Yang, O. Nachum, Y. Du, J. Wei *et al.*, "Foundation models for decision making: Problems, methods, and opportunities," 2023.

[21] H. Zhou, C. Hu, Y. Yuan, Y. Cui, Y. Jin, C. Chen, H. Wu, D. Yuan, L. Jiang, D. Wu *et al.*, "Large language model (llm) for telecommunications: A comprehensive survey on principles, key techniques, and opportunities," *IEEE Communications Surveys & Tutorials*, vol. 27, no. 3, pp. 1955–2005, 2024.

[22] N. Yang, M. Fan, W. Wang, and H. Zhang, "Decision-making large language model for wireless communication: A comprehensive survey on key techniques," *IEEE Communications Surveys & Tutorials*, 2025, early Access.

[23] M. Xu, D. Niyato, J. Kang, Z. Xiong *et al.*, "When large language model agents meet 6g networks: Perception, grounding, and alignment," *IEEE Wireless Communications*, 2024.

[24] Y. Zhao, Y. Yue, S. Hou, B. Cheng, and Y. Huang, "Lamosc: Large language model-driven semantic communication system for visual transmission," *IEEE Transactions on Cognitive Communications and Networking*, vol. 10, no. 6, pp. 2005–2018, 2024.

[25] X. Wu, J. Farooq, Y. Wang, and J. Chen, "Llm-xapp: A large language model empowered radio resource management xapp for 5g o-ran," in *Proceedings of the Symposium on Networks and Distributed Systems Security (NDSS), Workshop on Security and Privacy of Next-Generation Networks (FutureG 2025), San Diego, CA*, 2025.

[26] X. Zhang, J. Nie, Y. Huang, G. Xie, Z. Xiong, J. Liu, D. Niyato, and X. Shen, "Beyond the cloud: Edge inference for generative large language models in wireless networks," *IEEE Transactions on Wireless Communications*, vol. 24, no. 1, pp. 643–658, 2024.

[27] Z. Shao, P. Wang, Q. Zhu, R. Xu, J. Song, X. Bi, H. Zhang, M. Zhang, Y. Li *et al.*, "Deepseekmath: Pushing the limits of mathematical reasoning in open language models," *arXiv preprint arXiv:2402.03300*, 2024.

[28] B. Abolhassani, J. Tadrous, A. Eryilmaz, and E. Yeh, "Fresh caching of dynamic content over the wireless edge," *IEEE/ACM Transactions on Networking*, vol. 30, no. 5, pp. 2315–2327, 2022.

[29] N. Mhaisen, G. Iosifidis, and D. Leith, "Online caching with no regret: Optimistic learning via recommendations," *IEEE Transactions on Mobile Computing*, vol. 23, no. 5, pp. 5949–5965, 2023.

[30] L. Wang, Y. Wang, Z. Yu, F. Xiong, L. Ma, H. Zhou, and B. Guo, "Similarity caching in dynamic cooperative edge networks: An adversarial bandit approach," *IEEE Transactions on Mobile Computing*, 2024.

[31] J. Luo, Q. Wang, F.-C. Zheng, L. Gao, and S. Gu, "Cooperative activation and caching strategy for low-latency and energy-efficient small-cell networks," *IEEE Wireless Communications Letters*, vol. 11, no. 4, pp. 756–760, 2022.

[32] Z. Hu, C. Fang, R. Zhong, and Y. Liu, "Joint physical and network layers design for stars-assisted multi-cellular edge caching," *IEEE Transactions on Wireless Communications*, 2024.

[33] C. Zhong, M. C. Gursoy *et al.*, "Deep reinforcement learning-based edge caching in wireless networks," *IEEE Transactions on Cognitive Communications and Networking*, vol. 6, no. 1, pp. 48–61, 2020.

[34] H. Zhou, K. Jiang, S. He, G. Min, and J. Wu, "Distributed deep multi-agent reinforcement learning for cooperative edge caching in internet-of-vehicles," *IEEE Transactions on Wireless Communications*, vol. 22, no. 12, pp. 9595–9609, 2023.

[35] X. Zhou, Z. Ke, and T. Qiu, "Recommendation-driven multi-cell cooperative caching: A multi-agent reinforcement learning approach," *IEEE Transactions on Mobile Computing*, vol. 23, no. 5, pp. 4764–4776, 2023.

[36] Z. Zhang and M. Tao, "Deep learning for wireless coded caching with unknown and time-variant content popularity," *IEEE Transactions on Wireless Communications*, vol. 20, no. 2, pp. 1152–1163, 2020.

[37] X. Cheng, M. Gao, Q. Gao, and X.-H. Peng, "Impact of network settings on reinforcement learning based caching policy in cooperative edge networks," *ICT Express*, vol. 9, no. 6, pp. 1122–1127, 2023.

[38] D. Wu, X. Wang, Y. Qiao, Z. Wang, J. Jiang, S. Cui, and F. Wang, "Netllm: Adapting large language models for networking," in *Proceedings of the ACM SIGCOMM 2024 Conference*, 2024, pp. 661–678.

[39] A. Maatouk, N. Piovesan, F. Ayed, A. De Domenico, and M. Debbah, "Large language models for telecom: Forthcoming impact on the industry," *IEEE communications magazine*, 2024.

[40] R. Sutton and A. Barto, "Reinforcement learning: An introduction," *IEEE Transactions on Neural Networks*, vol. 9, no. 5, pp. 1054–1054, 1998.

[41] T. Dettmers, A. Pagnoni, A. Holtzman, and L. Zettlemoyer, "Qlora: Efficient finetuning of quantized llms," *Advances in neural information processing systems*, vol. 36, pp. 10 088–10 115, 2023.

[42] J. Schulman, F. Wolski, P. Dhariwal, A. Radford, and O. Klimov, "Proximal policy optimization algorithms," *arXiv preprint arXiv:1707.06347*, 2017.

[43] A. Y. Ng, D. Harada, and S. Russell, "Policy invariance under reward transformations: Theory and application to reward shaping," in *ICml*, vol. 99. Citeseer, 1999, pp. 278–287.

[44] B. Hui, J. Yang, Z. Cui, J. Yang, D. Liu, L. Zhang, T. Liu, J. Zhang, B. Yu, K. Lu *et al.*, "Qwen2. 5-coder technical report," *arXiv preprint arXiv:2409.12186*, 2024.

[45] M. Ahmed, S. Traverso, P. Giaccone, E. Leonardi, and S. Niccolini, "Analyzing the performance of lru caches under non-stationary traffic patterns," *arXiv preprint arXiv:1301.4909*, 2013.

[46] A. Jaleel, K. B. Theobald *et al.*, "High performance cache replacement using re-reference interval prediction (rip)," *ACM SIGARCH computer architecture news*, vol. 38, no. 3, pp. 60–71, 2010.

[47] D. Rossi and G. Rossini, "Caching performance of content centric networks under multi-path routing (and more)," *Relatório técnico, Telecom ParisTech*, vol. 2011, pp. 1–6, 2011.

[48] T. Haarnoja, A. Zhou, P. Abbeel, and S. Levine, "Soft actor-critic: Off-policy maximum entropy deep reinforcement learning with a stochastic actor," in *International conference on machine learning*. Pmlr, 2018, pp. 1861–1870.

APPENDIX A PROOF OF THEOREM 1

This appendix provides the detailed proof for the two properties claimed in Theorem 1. We demonstrate that maximizing the shaped reward is mathematically equivalent to maximizing the potential gain (Decision Invariance) and that the penalty mechanism strictly preserves the preference order among write actions while suppressing suboptimal passivity (Order Preservation).

A. Property 1: Decision Invariance

Fix a decision slot t and the frozen request window $\mathcal{Q}^{(t+1:t+H)}$ utilized by the look-ahead evaluator. Under the frozen-trajectory protocol, $\mathcal{Q}^{(t+1:t+H)}$ is exogenous and independent of the action chosen at slot t .

For any executable action a_t , let $\mathbf{X}^{(t+1)}(a_t)$ denote the cache configuration resulting from applying a_t to the current cache state $\mathbf{X}^{(t)}$. Define the augmented current state as $\bar{s}^{(t)} \triangleq (s_t, \mathcal{Q}^{(t+1:t+H)})$ and the post-action augmented state as $\bar{s}^{(t+1)}(a_t) \triangleq (s_{t+1}(a_t), \mathcal{Q}^{(t+1:t+H)})$. Note that the request window remains invariant because Eq. (15) evaluates both cache configurations against the same future sequence.

Given the potential function $\Phi(\bar{s}^{(t)}) \triangleq \mathcal{H}_H(\mathbf{X}^{(t)}; \mathcal{Q}^{(t+1:t+H)})$, we can rewrite the performance gain in Eq. (15) for any a_t as:

$$\Delta_{\text{perf}}(a_t) = \Phi(\bar{s}^{(t+1)}(a_t)) - \Phi(\bar{s}^{(t)}). \quad (23)$$

Since $\Phi(\bar{s}^{(t)})$ depends exclusively on the pre-decision cache state and the frozen request window, it is constant with respect to the optimization variable a_t . Consequently, the optimization objective simplifies as follows:

$$\begin{aligned} & \arg \max_{a_t} \Delta_{\text{perf}}(a_t) \\ &= \arg \max_{a_t} \left[\Phi(\bar{s}^{(t+1)}(a_t)) - \Phi(\bar{s}^{(t)}) \right] \\ &= \arg \max_{a_t} \Phi(\bar{s}^{(t+1)}(a_t)). \end{aligned} \quad (24)$$

This derivation confirms the decision invariance property: maximizing the shaped reward is equivalent to maximizing the potential of the next state.

B. Property 2: Order Preservation

We analyze the preservation of reward ranking through two distinct cases.

Case 1: Ranking between two write actions: Consider any two feasible write actions w_1 and w_2 . By definition, the penalty term satisfies $P_t(w_1) = P_t(w_2) = 0$. The difference in their shaped rewards is:

$$\tilde{R}_t(w_1) - \tilde{R}_t(w_2) = \Delta_{\text{perf}}(w_1) - \Delta_{\text{perf}}(w_2). \quad (25)$$

Thus, $\tilde{R}_t(w_1) > \tilde{R}_t(w_2)$ if and only if $\Delta_{\text{perf}}(w_1) > \Delta_{\text{perf}}(w_2)$, which implies that the preference ordering among write actions is strictly preserved.

Case 2: Strict demotion of NoOp : By definition, a NoOp action implies $\mathbf{X}^{(t+1)} = \mathbf{X}^{(t)}$, yielding $\Delta_{\text{perf}}(\text{NoOp}) = 0$. Assume there exists a write action w such that $\Delta_{\text{perf}}(w) > \Delta_{\text{perf}}(\text{NoOp}) = 0$.

- For the write action w :

$$\tilde{R}_t(w) = \Delta_{\text{perf}}(w) + P_t(w) = \Delta_{\text{perf}}(w) > 0. \quad (26)$$

- For the NoOp action: Since a superior write action exists (as identified by the expert), the opportunity penalty is triggered, i.e., $P_t(\text{NoOp}) = \lambda_{\text{opp}} < 0$. Thus:

$$\tilde{R}_t(\text{NoOp}) = 0 + P_t(\text{NoOp}) < 0. \quad (27)$$

Combining these results yields the strict inequality:

$$\tilde{R}_t(w) > 0 > \tilde{R}_t(\text{NoOp}). \quad (28)$$

This confirms that NoOp is strictly demoted relative to any write action that yields a positive performance gain. \blacksquare

APPENDIX B SCALABILITY OF JOINT EXHAUSTIVE SEARCH

Proposition 1 (Exponential growth of the joint action space). *At slot t , let $\mathcal{A}_{b,t}$ denote the feasible action set of BS b under the single-swap interface, and let \mathcal{A}_t denote the joint action space of all B BSs. The joint action space is defined as $\mathcal{A}_t = \prod_{b \in \mathcal{B}} \mathcal{A}_{b,t}$, with cardinality $|\mathcal{A}_t| = \prod_{b \in \mathcal{B}} |\mathcal{A}_{b,t}|$. If each BS admits at least one feasible write action in addition to NoOp (i.e., $|\mathcal{A}_{b,t}| \geq 2$ for all b), then $|\mathcal{A}_t| \geq 2^B$, implying that the complexity of joint exhaustive enumeration grows exponentially with the number of BSs.*

Proof. By definition, the controller outputs exactly one action per BS. Thus, a joint action is represented as the tuple:

$$a_t = (a_t^{(1)}, \dots, a_t^{(B)}), \quad \text{where } a_t^{(b)} \in \mathcal{A}_{b,t}. \quad (29)$$

Consequently, the joint feasible set is the Cartesian product of the individual feasible sets:

$$\mathcal{A}_t = \mathcal{A}_{1,t} \times \dots \times \mathcal{A}_{B,t} = \prod_{b \in \mathcal{B}} \mathcal{A}_{b,t}. \quad (30)$$

The cardinality of the joint action space is the product of the cardinalities of the individual action sets:

$$|\mathcal{A}_t| = \prod_{b \in \mathcal{B}} |\mathcal{A}_{b,t}|. \quad (31)$$

Given the condition that $|\mathcal{A}_{b,t}| \geq 2$ for all $b \in \mathcal{B}$, we derive the lower bound:

$$|\mathcal{A}_t| = \prod_{b \in \mathcal{B}} |\mathcal{A}_{b,t}| \geq \prod_{b \in \mathcal{B}} 2 = 2^B. \quad (32)$$

This exponential lower bound renders joint exhaustive search computationally intractable for large B . \square